Modelling approaches for atmospheric ion-dipole collisions: all-atom trajectory simulations and central field methods

Ivo Neefjes[1], Roope Halonen[2], Hanna Vehkamäki[1], and Bernhard Reischl[1]

[1]Institute for Atmospheric and Earth System Research / Physics, Faculty of Science, University of Helsinki, P.O. Box 64, FI-00014, Finland
[2]Center for Joint Quantum Studies and Department of Physics, School of Science, Tianjin University, 92 Weijin Road, Tianjin 300072, China

Correspondence: Ivo Neefjes (ivo.neefjes@helsinki.fi), Roope Halonen (roope@tju.edu.cn)

Abstract. Ion-dipole collisions can facilitate the formation of atmospheric aerosol particles, and play an important role in their detection in chemical ionization mass spectrometers. Conventionally, analytical models, or simple parametrizations, have been used to calculate rate coefficients of ion-dipole collisions in the gas phase. Such models, however, neglect the atomistic structure and charge distribution of the collision partners. To determine the accuracy and applicability of these approaches at atmospheric

5　conditions, we calculated collision cross sections and rate coefficients from all-atom molecular dynamics collision trajectories, sampling the relevant range of impact parameters and relative velocities, and from a central field model using an effective attractive interaction fitted to the long-range potential of mean force between the collision partners. We considered collisions between various atmospherically relevant molecular ions and dipoles, as well as charged and neutral dipolar clusters. Based on the good agreement between collision cross sections and rate coefficients obtained from molecular dynamics trajectories and a

10　generalized central field model, we conclude that the effective interactions between the collision partners are isotropic to a high degree, and the model is able to capture the relevant physico-chemical properties of the systems. In addition, when the potential of mean force is recalculated at the respective temperatures, the central field model exhibits the correct temperature dependence of the collision process. The classical parametrization by Su and Chesnavich [J. Chem. Phys., 76, 5183–5185, 1982], which combines a central field model with simplified trajectory simulations, is able to predict the collision rate coefficients and their

15　temperature dependence quite well for molecular systems, but the agreement worsens for systems containing clusters. Based on our results, we propose the combination of potential of mean force calculation and central field model as a viable and elegant alternative to brute force sampling of individual collision trajectories over a large range of impact parameters and relative velocities.

1 Introduction

20　In the atmosphere, gas-phase molecules can aggregate to form molecular clusters, and subsequently grow into larger sized atmospheric aerosol particles, in a process called new particle formation (NPF) (Gordon et al., 2017). Once formed, atmospheric aerosol particles affect the global climate both directly, by scattering and absorbing solar radiation, and indirectly, by acting as nuclei for the formation of clouds (Kurtén et al., 2003). Aerosol particles are, furthermore, responsible for adverse

health effects through air pollution (Falcon-Rodriguez et al., 2016). It is estimated that the majority of atmospheric aerosol
25 particles originates from NPF (Gordon et al., 2017; Yu and Luo, 2009). NPF is mainly driven by neutral pathways, involving
trace gas molecules such as sulfuric acid and various bases. The presence of atmospheric ions can, however, significantly en-
hance NPF (Kirkby et al., 2016; Wagner et al., 2017). Atmospheric ions are formed under the influence of galactic cosmic rays
and terrestrial radioactivity (Zhang et al., 2011), and stabilize newly formed atmospheric clusters. Ions, furthermore, play an
important role in the detection and characterization of atmospheric clusters through chemical ionization mass spectrometry,
30 which depends on collisions between the studied atmospheric clusters and ions to form detectable charged clusters (Zhao et al.,
2010).

The first stage of NPF is the gas-phase collision between single molecules or ions to form a dimer. For a theoretical de-
scription of NPF, it is therefore crucial to properly characterize the thermodynamics and kinetics of these initial collisions. In
current NPF models, the cluster thermodynamics (e.g., cluster binding free energies and therefrom derived fragmentation rate
35 coefficients) are treated with high-level quantum chemical calculations (Elm, 2019; Elm et al., 2020), whereas the treatment of
the cluster kinetics (e.g., collision cross sections and collision rate coefficients) is less sophisticated.

The theoretical prediction of collision kinetics is a long-standing topic throughout physics and chemistry (e.g., atmospheric
chemistry, subatomic physics, and mass spectrometry), and thus several theoretical and computational methods have been
developed. Collision rate coefficients generally depend on both the relative velocity between the collision partners and the fluid
40 density regime (Gopalakrishnan and Hogan Jr, 2011; Thajudeen et al., 2012). Here, we concentrate on methods developed
for resolving canonical collision rate coefficients (i.e., the velocities of the collision partners follow the Maxwell-Boltzmann
distribution) in the free molecular regime. An approximate estimate is obtained by assuming the collision partners to be non-
interacting hard spheres with well-defined radii. Although intermolecular interactions are ignored in this approach, the hard-
sphere model is widely used, especially for collisions between two neutral collision partners.

45 Neglecting the attractive forces between the collision partners can result in significant discrepancies with experiments,
especially for systems with strong intermolecular interactions, such as systems containing ions. In 1905, Langevin (1905)
derived an expression for the rate coefficient of a collision involving ion-neutral interactions using a central field approach.
Although Langevin derived a compact equation specifically for the collision rate coefficients of systems with an ion-induced
dipole interaction, later revisited by Gioumousis and Stevenson (Gioumousis and Stevenson, 1958), the central field approach
50 can be used with any attractive potential, e.g., for ion-"locked in" dipole (Moran and Hamill, 1963) and ion-averaged dipole
orientation (Su and Bowers, 1973; Su et al., 1978) models.

In addition, various statistical models (often referred to as variational transition state theories), with quantized energy levels,
exist for collision processes (Chesnavich et al., 1979, 1980; Troe, 1985, 1987; Clary, 1990; Georgievskii and Klippenstein,
2005). Interestingly, under equal assumptions, the statistical models give results identical to those of the central field models
55 (Chesnavich et al., 1979; Georgievskii and Klippenstein, 2005; Fernández-Ramos et al., 2006). One can also adopt a dynamical,
rather than a statistical, approach: the collision cross sections and rate coefficients can be obtained by numerically solving
the classical equations of motion with computational methods (Dugan Jr. and Magee, 1967; Chesnavich et al., 1980; Su and
Chesnavich, 1982; Maergoiz et al., 1996a, b, c; Yang et al., 2018; Halonen et al., 2019; Goudeli et al., 2020). Based on trajectory

simulations between a point-like charged particle and a polar rigid rod, Su and Chesnavich (1982) obtained a parametrized

60   model for the collision rate coefficient of ion-dipole collisions. This model has been shown to give rather good results for systems of small molecules and ions (Amelynck et al., 2005; Strekowski et al., 2019; Midey et al., 2001; Williams et al., 2004; Woon and Herbst, 2009), and is widely used in atmospheric sciences (e.g., in the Atmospheric Cluster Dynamics Code (McGrath et al., 2012)).

Although the aforementioned theoretical approaches are flexible and readily applicable, they often rely on simplified char-

65   acterizations of the studied collision system and the intermolecular interactions. This can potentially lead to significant inaccuracies in the predicted collision rate coefficients. As mentioned earlier, an ion-dipole complex is often reduced to a point-like charge and a polar rod. However, especially for larger molecules (or clusters), the non-symmetric molecular structure and dynamic partial charge distribution should be considered to determine the actual strength of the interaction. Recently, Halonen et al. (2019) compared collision rate coefficients obtained from the hard-sphere model and an atomistic molecular dynam-

70   ics (MD) model, including long range interaction, for a collision between two sulfuric acid molecules. The atomistic model showed an enhancement of the collision rate coefficient by a factor 2.2. This enhancement factor is close to the discrepancy between particle formation rates in experiments and a kinetic model reported by Kürten et al. (2014).

In this study, we examine collisions between one charged and one neutral dipolar collision partner. While there are typically significantly less ions present compared to neutral molecules, ion-neutral collision rate coefficients are higher than for neutral-

75   neutral collisions due to relatively strong long-range interactions. Such collisions usually do not involve a significant electronic activation energy barrier. However, the collision process does involve a *centrifugal barrier* due to the conservation of the system's angular momentum which can lead to interesting, non-standard, temperature dependencies (Clary, 1990).

Here, as test systems, we considered collisions of the atmospherically relevant molecular dipole sulfuric acid (H_2SO_4), with the anions bisulfate (HSO_4^-) and nitrate (NO_3^-), as well as the cations ammonium (NH_4^+) and dimethylammonium

80   ($(CH_3)_2NH_2^+$). To study the effect of an increase in the size of the ion, we considered collisions between H_2SO_4 and the sulfuric acid-bisulfate dimer ($[H_2SO_4 \cdot HSO_4^-]$). Likewise, to examine the effect of an increase in size of the dipole, we studied collisions of the neutral bisulfate-dimethylammonium dimer with HSO_4^- and $(CH_3)_2NH_2^+$. Lastly, we also looked at the dimer-dimer collision between $[HSO_4^- \cdot (CH_3)_2NH_2^+]$ and $[H_2SO_4 \cdot HSO_4^-]$.

We carried out all-atom MD trajectory simulations of the collisions to determine the collision rate coefficient directly from

85   the collision probabilities in relevant ranges of the impact parameter and relative velocity. Additionally, we calculated the potentials of mean force (PMF) between collision partners from well-tempered metadynamics simulations to determine the *effective* potential, arising from the same underlying atomistic interactions, at finite temperature. Attractive interactions fitted to the tail of the PMFs were used to predict collision cross sections and canonical rate coefficients using a central field model. Lastly, we compared the analytical Langevin-Gioumousis-Stevenson model and the parametrization of Su and Chesnavich to

90   our robust atomistic MD results, and assessed the accuracy and applicability of those theoretical approaches.

The remainder of this paper is organized as follows: in Sect. 2 we present and discuss the different theoretical models, the atomistic models of atmospherically relevant ions and dipoles studied, the PMF calculations, and the MD collision simulations. In Sect. 3, we report and compare the results using the central field model based on the PMF, the MD trajectory simulations,

as well as the Langevin-Gioumousis-Stevenson model and Su and Chesnavich parametrization, for the same atomistic model
95 systems. In Sect. 4, we summarize our results and conclude the paper.

2   Theory and Methods

The formation of a molecular cluster through collisions requires asymptotic attractive intermolecular interaction potentials
which can be ideally modelled as a function of the distance r, separating the two collision partners:

$$U(r) = -A\left(\frac{r}{r_0}\right)^a,\tag{1}$$

100 where A is an interaction coefficient, r_0 is a distance parameter, and $a < 0$ is the characteristic interaction exponent. The
collision cross section and collision rate coefficient in an isotropic potential field given by Eq. (1) can be solved analytically
for collisions between point-like particles.

In the central field model, one of the collision partners is set to be stationary while the other approaches from infinitely far
away with some initial velocity v_0. The perpendicular distance between the initial trajectory and the center of the field is called
105 the impact parameter b. The initial configuration is illustrated in Fig. 1. As the collision partners form an isolated system, both
energy (initially only kinetic energy) and angular momentum, $\mu v_0 b$, are conserved, and the following equality holds during the
trajectory:

$$\frac{1}{2}\mu v_0^2 = U(r) + \frac{\mu v_0^2 b^2}{2r^2} + \frac{1}{2}\mu v^2.\tag{2}$$

Here, μ is the reduced mass of the partners and v the instantaneous velocity. The effective potential $U(r) + \mu v_0^2 b^2/2r^2$ in-
110 troduces a centrifugal energy barrier between the two collision partners (see Fig. 1). Since the kinetic energy $\mu v^2/2 \geq 0$, the
following condition must hold:

$$U(r) + \frac{\mu v_0^2 b^2}{2r^2} - \frac{1}{2}\mu v_0^2 \leq 0.\tag{3}$$

The left hand side of Eq. (3) has its maximum at

$$r = \left(-\frac{\mu v_0^2 b^2 r_0^a}{Aa}\right)^{1/(2+a)}.\tag{4}$$

115 If the incoming collision partner can cross this critical distance, where the centrifugal barrier has its maximum, a collision
leading to cluster formation will occur.

Inserting Eq. (4) into Eq. (3), we obtain the maximum impact parameter $b_{\max}$ for which a collision is still possible, which
can then be used to express the collision cross section Ω_{CF} in an ideal, isotropic, central field as

$$\Omega_{\mathrm{CF}}(v_0) = \pi b_{\max}^2 = \frac{\pi a}{a+2}\left(-\frac{\mu v_0^2}{A(a+2)}\right)^{2/a} r_0^2.\tag{5}$$
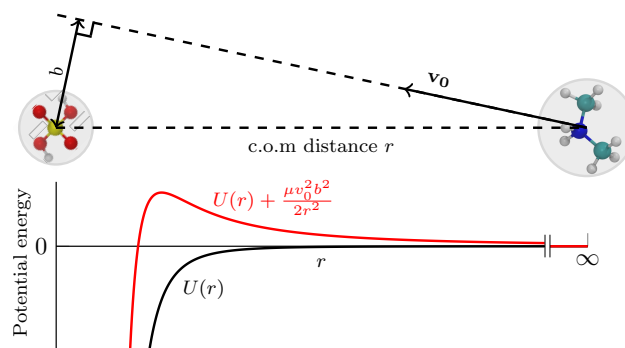
Figure 1. A schematic diagram of the central field approach with the corresponding potential energy profile. The molecule on the left is at rest and its center of mass (c.o.m.; center of the gray circle) designates the center of the field, while the molecule on the right initially moves along a trajectory set by velocity vector $\mathbf{v_0}$. At the start, the colliding molecules are infinitely far away from each other and the intermolecular potential energy $U(r)$ (black curve) equals zero. The perpendicular distance between the trajectory and the center of the field is the impact parameter b. If $b > 0$, the orbital angular momentum gives rise to a centrifugal barrier shown by the red curve.

120 In thermal equilibrium, the initial velocity v_0 follows the Maxwell-Boltzmann distribution, $f_{\mathrm{MB}}(v)$. For interaction exponent $a < -2$, the collision rate coefficient β_{CF} in a central field can be calculated as

$$
\begin{aligned}
\beta_{\mathrm{CF}}(T) &= \int_0^\infty \mathrm{d}v_0 \, v_0 f_{\mathrm{MB}}(v_0) \Omega_{\mathrm{CF}}(v_0) \\
&= \pi r_0^2 \sqrt{\frac{8k_{\mathrm{B}}T}{\pi\mu}} \Gamma\left(\frac{2+a}{a}\right) \left(-\frac{2k_{\mathrm{B}}T}{A(a+2)}\right)^{2/a},
\end{aligned}
\tag{6}
$$

where k_{B} is the Boltzmann constant, T is the temperature, and $\Gamma(x)$ denotes the Gamma function of x.

125 The presented central field model is essentially *adiabatic*; it is assumed that there is no exchange of energy between rotational and vibrational modes of the collision partners, or exchange of angular momentum between the rotations of the collision partners and the orbiting motion of the system as a whole (Su and Bowers, 1973). For actual chemical compounds with internal structures, strong interactions can affect the rotational motion of the molecules which effectively changes the height of the centrifugal barrier as the angular momentum of the system is conserved.

130 The expressions for both the collision cross section and rate coefficient are derived for a general, well-behaving, asymptotic attractive interaction given by Eq. (1), and hence Eqs. (5) and (6) are convenient expressions to analyze and characterize the collision dynamics. In addition, two well-known results can be directly derived from Eq. (6): (1) When the interaction exponent a approaches $-\infty$, the rate coefficient β_{CF} reduces to the kinetic gas theory result for two hard spheres of radii R_i and R_j:

$$
\beta_{\mathrm{HS}}(T) = \pi(R_i + R_j)^2 \sqrt{\frac{8k_{\mathrm{B}}T}{\pi\mu}}.
\tag{7}
$$

135 (2) The main contribution to the intermolecular interactions for collisions between an ion and neutral particle is the ion-induced dipole interaction,

$$U(r) = \frac{\alpha q^2}{2r^4}, \tag{8}$$

where q is the charge of the ion and α is the angle-averaged polarizability of the dipole. For such an interaction, Eq. (6) becomes

140
$$\beta_{\mathrm{L}} = 2\pi q \sqrt{\frac{\alpha}{\mu}}. \tag{9}$$

This is known as the Langevin-Gioumousis-Stevenson expression (Langevin, 1905; Gioumousis and Stevenson, 1958). Note that the temperature dependency of β_{L} vanishes because the interaction exponent $a = -4$ in Eq. (8).

2.1 Su and Chesnavich parametrization

For collisions between an ion and polar neutral compound, angle-dependent ion-permanent dipole interactions should also be
145 considered. In the most extreme case, the orientation of the dipole can be "locked in" so that the strength of the interaction is maximized. While thermal rotations of the collision partners will often prevent the dipole from "locking in", the ion-permanent dipole interaction is not necessarily averaged over all angles. Su and Chesnavich (1982) performed classical trajectory simulations of collisions between a point charge and a polarizable two-dimensional rigid rotor. Based on these findings, they developed a parametrized correction to the Langevin-Gioumousis-Stevenson expression (Eq. (9)):

150
$$\beta_{\mathrm{SC}} = K\beta_{\mathrm{L}}. \tag{10}$$

The correction term, K, depending only on the temperature, polarizability α, and dipole moment μ_{D}, was found to be (Su and Chesnavich, 1982)

$$K = \begin{cases} 0.4767x + 0.6200; & x \geq 2, \\ \frac{(x + 0.5090)^2}{10.526}; & x \leq 2 \end{cases} \tag{11}$$

with

155
$$x = \frac{\mu_{\mathrm{D}}}{(2\alpha k_{\mathrm{B}}T)^{1/2}}. \tag{12}$$

Su and Chesnavich observed that for all realistic systems, K does not depend on the moments of inertia of the collision partners (Su and Chesnavich, 1982). Note that Eqs. (8)–(12) are written for Gaussian cgs units.

Maergoiz et al. (1996a) later validated Eq. (11) with their independent trajectory study of a similar system.

2.2 Atomistic model of ion-dipole systems

160 #### 2.2.1 Collision systems

We studied a total of eight ion-dipole collision systems. Systems with only molecular ions and dipoles were studied, as well as systems with either a dipolar or charged dimer, or both. For five of the systems, sulfuric acid (H_2SO_4) served as the molec-
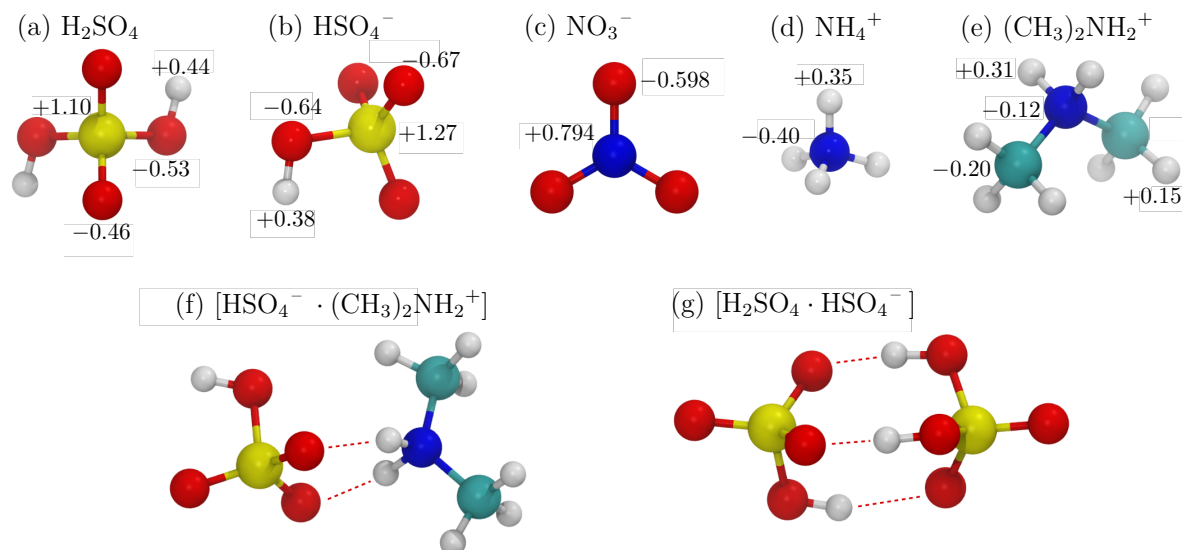
Figure 2. Stick-and-ball representations of the studied dipoles and ions: (a) sulfuric acid molecule, (b) bisulfate, (c) nitrate, (d) ammonium, (e) dimethylammonium ions, (f) neutral bisulfate-dimethylammonium dimer, and (g) charged sulfuric acid-bisulfate dimer. Atom partial charges according to the force field are indicated in panels a-e. The color codes of the atoms are as follows: sulfur–yellow, oxygen–red, nitrogen–blue, carbon–cyan, and hydrogen–white. Hydrogen bonds in the dimer structures (f,g) are indicated by dashed red lines.

ular dipole, while the ion was (1) bisulfate (HSO_4^-), (2) nitrate (NO_3^-), (3) ammonium (NH_4^+), (4) dimethylammonium ((CH_3)$_2NH_2^+$), and (5) the sulfuric acid-bisulfate dimer ([$H_2SO_4 \cdot HSO_4^-$]). The remaining three systems had the bisulfate-

165 dimethylammonium dimer ([$HSO_4^- \cdot (CH_3)_2NH_2^+$]) as a dipolar dimer. For these three systems, the ions were (1) HSO_4^-, (2) (CH_3)$_2NH_2^+$, and (3) [$H_2SO_4 \cdot HSO_4^-$]. The ions and dipoles of the studied systems are illustrated in Fig. 2 and their key physical properties are provided in Appendices A and B.

2.2.2 Force field

To describe the test systems, we employed a force field fitted according to the OPLS all-atom procedure (Jorgensen et al.,

170 1996). In the OPLS force field, the intramolecular interactions consist of harmonic bond potentials between covalently bonded atoms, harmonic angle potentials between atoms separated by two covalent bonds, and dihedral angle potentials between atoms separated by three covalent bonds,

$$U_{intra}^{OPLS} = \sum_{i=1}^{N_{bonds}} \frac{k_i^b}{2} \left(r_i - r_i^0 \right)^2 + \sum_{j=1}^{N_{angles}} \frac{k_j^\theta}{2} \left(\theta_j - \theta_j^0 \right)^2$$
$$+ \sum_{k=1}^{N_{dihedrals}} \sum_{n=1}^{4} \frac{V_n}{2} \left[1 + \cos \left(n\phi^k - \phi_n^k \right) \right], \tag{13}$$

175   where k_i^{b}, r_i, and r_i^0 are the force constant, instantaneous, and equilibrium length of bond i, k_j^θ, θ_j, and θ_j^0 are the force

constant, instantaneous, and equilibrium value of angle j, and V_n, ϕ_n^k, and ϕ^k are the Fourier coefficients, phase angles, and

instantaneous value of the dihedral angle k.

The intermolecular interactions, as well as intramolecular interactions between atoms separated by more than three covalent

bonds, are described by Lennard-Jones potentials between atoms i and j separated by a distance r_{ij}, with distance and energy

180   parameters σ_{ij} and ϵ_{ij}, and Coulomb interactions between the atoms' partial charges q_i and q_j,

$$
U_{\mathrm{inter}} = \sum_{i=1}^{N_1} \sum_{j=1}^{N_2} 4\epsilon_{ij} \left[\left(\frac{\sigma_{ij}}{r_{ij}} \right)^{12} - \left(\frac{\sigma_{ij}}{r_{ij}} \right)^6 \right]
$$
$$
+ \sum_{i=1}^{N_1} \sum_{j=1}^{N_2} \frac{1}{4\pi\epsilon_0} \frac{q_i q_j}{r_{ij}}, \tag{14}
$$

where ϵ_0 is the vacuum permittivity.

The OPLS force field parameters used in this study were obtained from Loukonen et al. (2014) for H_2SO_4, HSO_4^-, and

185   $(CH_3)_2NH_2^+$ and from Mosallanejad et al. (2020) for NO_3^- and NH_4^+. We note that in the original OPLS force field, Lennard-

Jones and Coulomb interactions between atoms separated by three covalent bonds ("1-4 interactions") are scaled by a factor

0.5. Loukonen et al. set this scaling factor to zero when fitting the force field parameters. For consistency, we have also set

these interactions to zero in our simulations. The optimized geometry of the studied ions and dipoles described by the OPLS

force field showed only minimal differences compared to *ab initio* geometries, obtained at the ωB97X-D/6-31++G** level of

190   theory, taken from Elm (2019). Using the OPLS force field, we obtained dipole moments $\mu_{\mathrm{D}}^{\mathrm{OPLS}} = 3.17$ and 13.20 Debye,

and polarizabilities $\alpha^{\mathrm{OPLS}} = 6.57$ and 7.91 Å^3, for H_2SO_4 and $[HSO_4^- \cdot (CH_3)_2NH_2^+]$, respectively. The agreement of these

values with *ab initio* calculations is very good for H_2SO_4 and reasonable for $[HSO_4^- \cdot (CH_3)_2NH_2^+]$. The details of the dipole

moment and polarizability calculations, as well as a benchmark of cluster binding energies, from *ab initio* and using the OPLS

force field, are provided in Appendices A and B.

195   **2.3   Potential of Mean Force**

Temperature-dependent long-range attractive interactions and binding free energies of the ion-dipole systems can be obtained

from the potential of mean force (PMF) as a function of the distance r between the ion and the dipole. The PMF differs

from the Helmholtz free energy profile by a term $-k_{\mathrm{B}}T\ln r^2$, which accounts for the configurational entropy of the system.

PMFs were calculated with the well-tempered metadynamics method (Barducci et al., 2008), where the energy surface of a

200   system is explored along one or more collective variables (CVs). In order to explore the CV space systematically, during a

molecular dynamics (MD) run, Gaussian energy packets are deposited at certain time intervals to make often visited regions

around the energy minima less favorable. Eventually, the sum of the Gaussian packages converges to the negative of the PMF.

In well-tempered metadynamics simulations, the height of the Gaussian packages is decreased over time to ensure proper

convergence.

205   We ran well-tempered metadynamics simulations using the LAMMPS code (Plimpton, 1995) together with the PLUMED plug-in (Tribello et al., 2014). For each system, the distance between the centers of mass of the collision partners was used as the collective variable. To confine the systems to the non-asymptotic region of the PMF, harmonic upper walls along the CV at 32 Å, or 50 Å, were used for systems containing only molecular ions and dipoles, or at least one dimer, respectively. No cut-off was used for the Lennard-Jones and Coulomb potentials over the allowed range of the CV. To ensure that the dimer structures

210   remained intact during the PMF calculation, appropriate harmonic upper walls were also applied to the center-of-mass distance between their constituents. To speed up the calculations, we used 40 random walkers dropping Gaussian energy packages every 0.5 ps. For all systems, the energy packages had an initial width of 0.1 Å and initial height of k_BT and the bias factor was 25, except for the two most weakly binding systems, $H_2SO_4 - NH_4^+$ and $H_2SO_4 - (CH_3)_2NH_2^+$, where the initial height was $0.5k_BT$ and the bias factor 15. We employed a Velocity Verlet integrator with a time step of 1 fs for a total simulation time of

215   4 ns per walker. A stochastic velocity rescaling thermostat with a time constant of 0.1 ps was used to maintain a temperature of $T = 300$ K. For the $H_2SO_4 - HSO_4^-$ system, PMF calculations were also carried out at $T = 200$ and 400 K, otherwise using similar well-tempered metadynamics parameters.

2.4   Molecular Dynamics collision simulations

To obtain ion-dipole collision cross sections and rate coefficients from MD simulations, we determined the collision probability

220   over a relevant range of impact parameters and relative velocities. All collision simulations were carried out with the LAMMPS code (Plimpton, 1995). At the start of the simulation, the collision partners were placed 600 Å apart along the x-axis, well beyond the cut-off of the Lennard-Jones and Coulomb potentials of the OPLS force field at 280 Å. The collision partners were first separately equilibrated for 50 ps using a Langevin thermostat with a damping factor of 0.1 ps. During the equilibration, both the center-of-mass motion of each collision partner and the angular momentum of the total system were removed. A

225   thorough analysis of different thermostats revealed that, for the studied flexible compounds, the Langevin thermostat is best suited to ensure equipartition of rotational and vibrational energies. Details of these investigations will be published elsewhere (Halonen et al., 2022). After the equilibration, the distance between the now orientationally randomized collision partners was decreased to 200 Å along the x-axis, bringing them within range of the long-range intermolecular potentials for impact parameters $b \lesssim 190$ Å. Both collision partners were then given a velocity along the x-direction of $v_x = \pm v_0/2$ towards each

230   other, where v_0 is the initial relative velocity. For each system, the range of relative velocities started at 50 ms^{-1} and increased in steps of 50 ms^{-1}. The highest relative velocity was determined so that at least 99% of the Maxwell-Boltzmann distribution was sampled. We sampled impact parameters starting from 0 Å up to the first impact parameter for which the collision probability at all sampled relative velocities was zero, in steps of 1 Å along the z-axis.

   Collisions were determined based on the minimum center-of-mass distance between the collision partners during the tra-

235   jectory. All collisions were simulated in the NVE ensemble, with an initial thermal energy corresponding to a temperature of 300 K achieved during equilibration. In addition, we studied the temperature dependence of the collision probability for the $H_2SO_4 - HSO_4^-$ system. We employed a Velocity Verlet integrator with a time step of 1 fs. The duration of the simulation was dependent on the initial relative velocity. It was determined as the time it would take for two non-interacting particles to
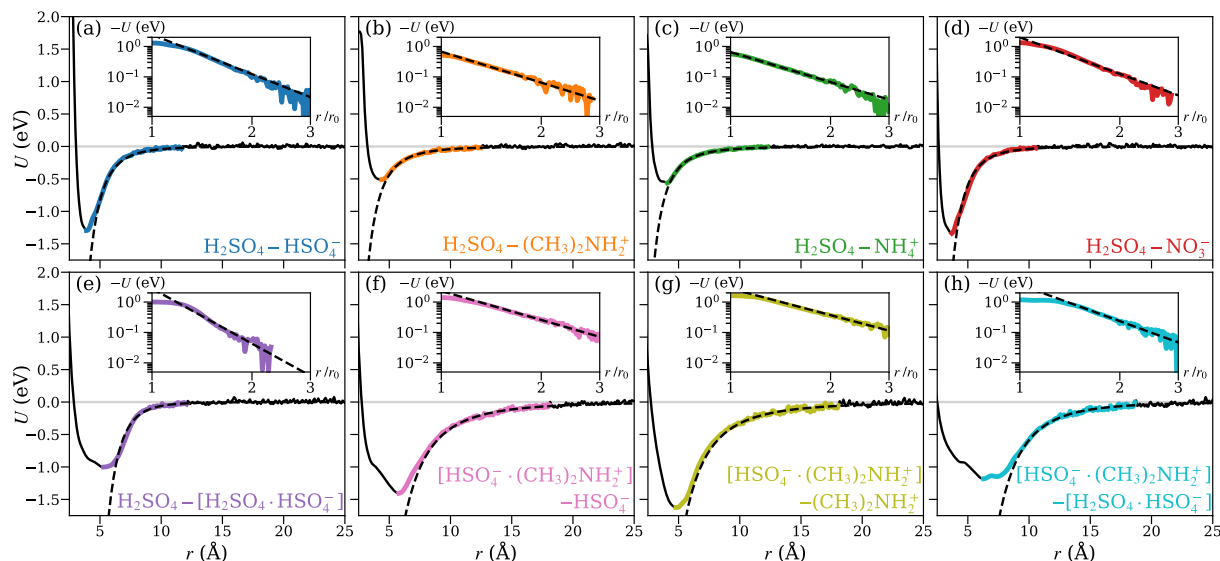
Figure 3. The potential of mean force (PMF) along the center-of-mass distance between the collision partners for the systems of H_2SO_4 and (a) HSO_4^-, (b) $(CH_3)_2NH_2^+$, (c) NH_4^+, (d) NO_3^- (top row), and (e) H_2SO_4 and the $[H_2SO_4 \cdot HSO_4^-]$ dimer, the $[HSO_4^- \cdot (CH_3)_2NH_2^+]$ dimer and (f) HSO_4^-, (g) $(CH_3)_2NH_2^+$, (h) the $[H_2SO_4 \cdot HSO_4^-]$ dimer (bottom row). The solid black lines show the PMF curves obtained from well-tempered metadynamics simulations. The range over which the attractive interaction is fitted using Eq. (1) is highlighted in color, and shown on a logarithmic scale in the insets. The fits are shown as dashed black lines.

cross each other plus 50 ps. For each combination of relative velocity and impact parameter, 1000 independent trajectories
240 were simulated to obtain a statistically significant estimate of the collision probability.

3 Results and Discussion

3.1 Long-range attractive interactions fitted to the potential of mean force

Figure 3 shows the potentials of mean force (PMF) as a function of the center-of-mass distance between the collision partners, for the eight studied systems, obtained from well-tempered metadynamics simulations. We fitted the general intermolecular
245 interaction potential of Eq. (1) to each of the PMF curves. The distance parameter r_0 was set to the location of the minimum of the PMF curve. It should be noted that for the long-range attractive tail of the potential, this choice does not influence the final results when applying the central field model as r_0 only affects the coefficient A, while leaving the exponent a unaltered. The attractive interaction was fitted to the range at which $U(r)$ is continuously negative and $r > r_0$, shown in the insets of Fig. 3 on logarithmic scale, so that the slope of the inset curve, $\ln(-U)$, is the interaction parameter a and the y-intersect is $\ln A$. The
250 fitted values of the interaction parameters r_0, A, and a are summarized in Tab. 1.

Table 1. The location of the potential minimum r_0, the interaction coefficient A, and the interaction exponent a, obtained by fitting Eq. (1) to the potential of mean force, as well as the reduced mass μ and the x parameter in the Su and Chesnavich parametrization, for each studied ion-dipole system.

System	r_0 (Å)	A (eV)	a	μ (amu)	x
$H_2SO_4 - HSO_4^-$	3.89	2.45	-4.31	48.75	4.30
$H_2SO_4 - NO_3^-$	3.69	2.00	-4.00	37.98	4.30
$H_2SO_4 - (CH_3)_2NH_2^+$	4.39	0.68	-3.38	31.31	4.30
$H_2SO_4 - NH_4^+$	4.09	0.65	-3.27	15.21	4.30
$H_2SO_4 - [H_2SO_4 \cdot HSO_4^-]$	5.29	2.78	-6.01	65.22	4.30
$[HSO_4^- \cdot (CH_3)_2NH_2^+] - HSO_4^-$	5.79	2.31	-3.16	57.80	18.52
$[HSO_4^- \cdot (CH_3)_2NH_2^+] - (CH_3)_2NH_2^+$	4.79	2.77	-2.90	34.80	18.52
$[HSO_4^- \cdot (CH_3)_2NH_2^+] - [H_2SO_4 \cdot HSO_4^-]$	6.28	3.71	-3.98	82.50	18.52

The fitted attractive interactions reveal interesting differences between the systems. The interactions between sulfuric acid (H_2SO_4) and the two anions are much stronger than with the two cations, in agreement with preliminary *ab initio* calculations (see Tab. B1). In addition, the exponent of the fitted interaction is close to -4 for the anions, similar to rotationally averaged ion-(induced) dipole interactions, but closer to -3 for the cations. The systems involving at least one dimer all exhibit strong

255   attractive interactions with interaction exponents between -3 and -6, indicating that those interactions are more complex, with the latter value resembling the standard interaction potential between permanent or induced dipoles. We note that for most systems considered here, the fitted effective interactions cannot be described by the standard ion-induced dipole, or ion-permanent dipole potential alone, but are a linear combination of different types of atomistic pair potentials.

3.2   Collision probability distributions and cross sections

260   Figures 4(a–d) and 5(a–d) show heat maps of the collision probabilities $P(v,b)$ obtained from the molecular dynamics (MD) collision simulations for molecular ion-dipole systems, and systems containing at least one dimer, respectively. The center-of-mass distance criterion for a successful collision was determined for each system by taking the distance at which the value of the PMF was $5k_BT$ (~ 0.13 eV at 300 K) higher than its minimum, to account for thermal fluctuations. We tested multiple criteria for determining collisions, and found them to be quite robust. However, the chosen criterion was deemed the most

265   physically intuitive, as we are not interested in distinguishing between collisions and "sticking" in this work.

    Unlike in the PMF calculations, no constraints were imposed on center-of-mass distances within the dimer structures $[H_2SO_4 \cdot HSO_4^-]$ and $[HSO_4^- \cdot (CH_3)_2NH_2^+]$ in the MD collision simulations. In every single MD simulation, these dimers remained intact during equilibration. Evaporations of the original dimers after the collision were only observed for the $[HSO_4^- \cdot (CH_3)_2NH_2^+]$ dimer in a certain window of impact parameters at high relative velocities. By far the highest evaporation probability observed

270   was ~ 3 % for the $[HSO_4^- \cdot (CH_3)_2NH_2^+] - HSO_4^-$ system at $v = 1000$ ms^{-1} and $b = 16$ Å. All collision trajectories resulting
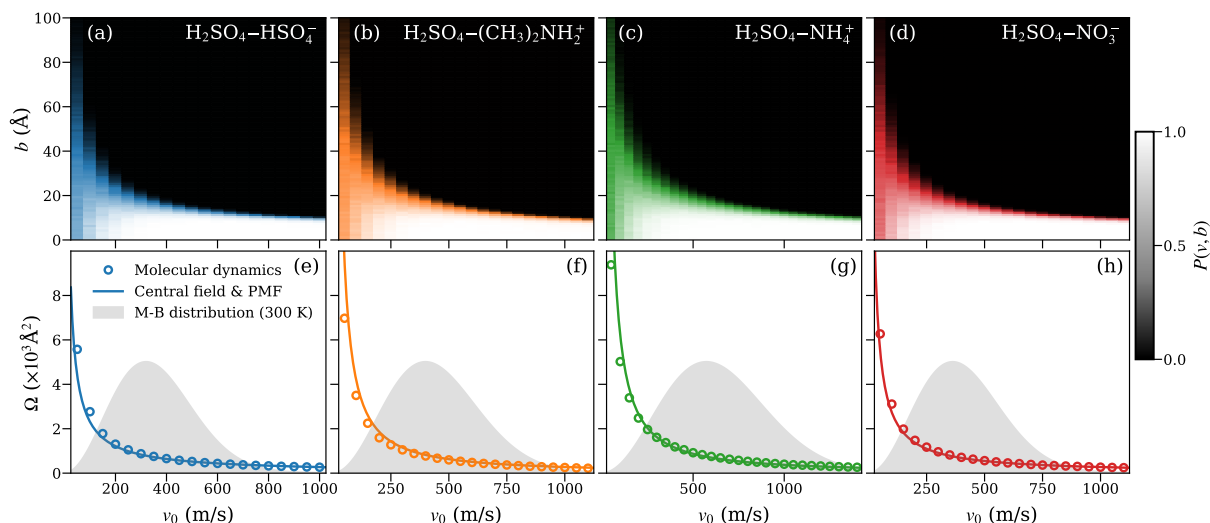
Figure 4. Heat maps of the collision probabilities from molecular dynamics (MD) for molecular ion-dipole systems as a function of initial relative velocity v_0 and impact parameter b (a–d, top row). Corresponding dynamic collision cross sections $\Omega_{\mathrm{MD}}(v)$ obtained from these MD collision probabilities (open circles) and collision cross sections $\Omega_{\mathrm{CF}}(v)$ based on the central field model (solid lines) using an attractive interaction fitted to the PMF (e–h, bottom row). The Maxwell-Boltzmann distribution of the relative velocity for each system is indicated by the gray area.

in an evaporation of the original dimer were discarded and additional simulations carried out to ensure a valid sample size of 1000 for each combination of relative velocity and impact parameter.

The collision probability heat maps all exhibit similar dependencies on v and b: for large relative velocities, the collision probability is unity at small impact parameters $b \lesssim 10$ Å, and drops sharply to zero when b increases. As the relative velocity decreases, the decline in collision probability is shifted to larger values of b, while at the same time becoming more gradual as a function of b. At small relative velocities ($v_0 \lesssim 200$ ms^{-1}), we observe collision probabilities significantly lower than one for small values of b, while small, but non-zero collision probabilities persist up to large values of b. This effect is especially significant at the lowest values of v_0 considered, where the collision probability at $b = 0$ Å, is typically only ~ 0.5, but non-zero collision probabilities remain even past $b = 100$ Å. The reduced collision probabilities at low values of v_0 is caused by small oscillations in the interaction energy, at large separation distances and periodic in time, which can lead to repulsion between the collision partners, as previously shown for dipole-dipole collisions (Halonen et al., 2019).

The dynamic collision cross section is a measure for the velocity dependent collision probability over all impact parameters considered in the MD simulations, and can be calculated as

$$\Omega_{\mathrm{MD}}(v) = \pi \int_{0}^{\infty} \mathrm{d}b^2 \, P(v, b). \tag{15}$$
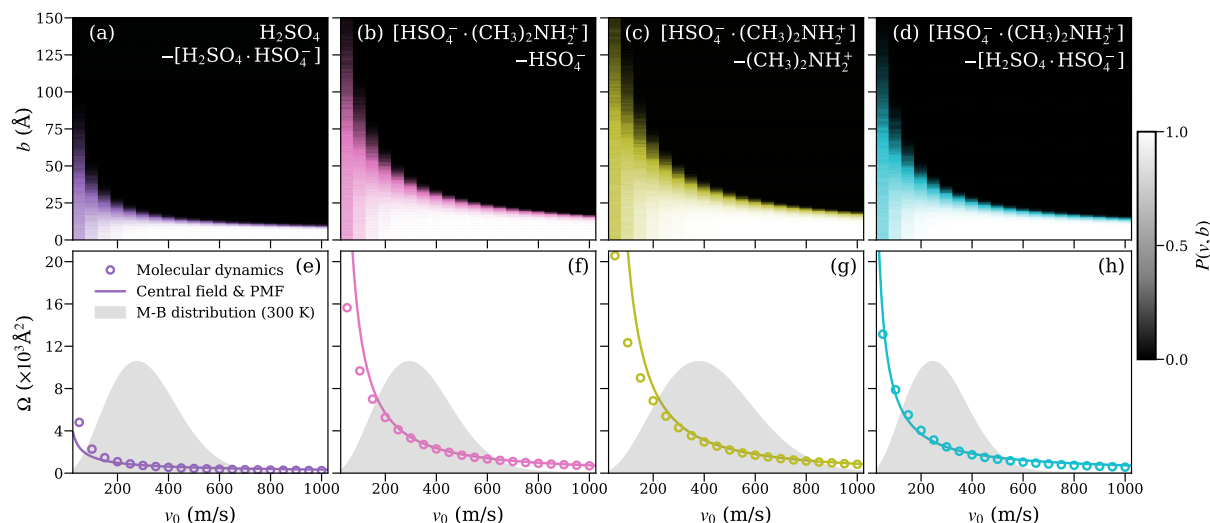
Figure 5. Heat maps of the collision probabilities from molecular dynamics (MD) for ion-dipole systems including at least one dimer as a function of initial relative velocity v_0 and impact parameter b (a–d, top row). Corresponding dynamic collision cross sections $\Omega_{MD}(v)$ obtained from these MD collision probabilities (open circles) and collision cross sections $\Omega_{CF}(v)$ based on the central field model (solid lines) using an attractive interaction fitted to the PMF (e–h, bottom row). The Maxwell-Boltzmann distribution of the relative velocity for each system is indicated by the gray area.

285 Figures 4(e–h) and 5(e–h) show the collision cross section obtained from the MD collision simulations of molecular systems, and systems containing at least one dimer, respectively, as circles. The collision cross section from the central field model, evaluated using Eq. (5) with parameters r_0, A, and a, obtained from the fit to the PMF curve of the system, is given by the solid line. For the molecular ion-dipole systems, we find excellent agreement between collision cross sections obtained from the collision MD simulations and from the central field model using the fit to the PMF, over the entire range of relative velocities.

290 For the systems containing at least one dimer, the agreement between the two approaches is still good, in particular over the most relevant velocity range according to the Maxwell-Boltzmann distribution.

This agreement indicates that the framework of the central field model adequately captures the underlying atomistic collision dynamics of the studied ion-dipole systems. As the model assumes point-like, structureless collision partners, it disregards any energy transfer between the partners' respective internal degrees of freedom and the orbiting motion of the system as a

295 whole. As a result, the centrifugal barrier is solely determined by the system's initial orbital angular momentum. Based on the demonstrated predictive power of Eq. (5), the assumption of adiabaticity (i.e., that the motion of the orbiting system as a whole is well-separated from the intramolecular motion of the collision partners) is well justified here. Furthermore, the results imply that the effective field of attraction is isotropic and can be described by simple interaction parameters, even for collision partners with complex and dynamic charge distributions, such as the $[HSO_4^- \cdot (CH_3)_2NH_2^+] - [H_2SO_4 \cdot HSO_4^-]$ system.

3.3 Canonical collision rate coefficients

The canonical collision rate coefficient can be calculated from the effective collision cross section of Eq. (15) as

$$\beta_{\mathrm{MD}} = \pi \int \mathrm{d}v \, v f_{\mathrm{MB}}(v) \Omega_{\mathrm{MD}}(v). \tag{16}$$

Table 2 shows the collision rate coefficients, obtained from the MD collision simulations β_{MD} in Eq. (16), the central field model with interaction parameters fitted to the PMF curve β_{CF} in Eq. (6), the Langevin-Gioumousis-Stevenson model β_{L} in Eq. (9), and the Su and Chesnavich parametrization β_{SC} in Eq. (11), for all studied systems. Overall, we find collision rate coefficients of similar magnitudes for the systems containing a molecular dipole. In comparison, systems containing a dipolar dimer exhibit larger collision rate coefficients as well as more variation in magnitude between the systems. We find excellent agreement within 10 % across all systems for the collision rate coefficients obtained from MD and the central field model using the interactions obtained from the PMF calculation. This indicates that collisions dynamics are indeed well captured by an adiabatic model and isotropic interactions.

The Langevin-Gioumousis-Stevenson model performs quite poorly with collision rate coefficients deviating by a factor of three for systems with a molecular dipole and a factor larger than 12 for systems containing a dipolar dimer. In comparison, the Su and Chesnavich parametrization is in quite good agreement with the MD or central field results, underestimating the collision rate coefficients by 10–20 % for systems containing H_2SO_4 as the dipole, and 30–40 % for systems containing $[HSO_4^- \cdot (CH_3)_2NH_2^+]$. The Su and Chesnavich parametrization differs from the Langevin-Gioumousis-Stevenson expression in two ways: first, in addition to the polarizability it also takes into account the permanent dipole moment of the neutral collision partner. Second, the thermal correction factor, obtained by Su and Chesnavich from trajectory simulations, adds a dependence on temperature to account for the dynamics of the rotating dipole. This significantly improves the accuracy of the model compared to the Langevin-Gioumousis-Stevenson expression and explains the rather good agreement with the all-atom molecular dynamics simulations in this work. However, we expect the discrepancies to increase for more complex systems.

Due to the Maxwell-Boltzmann distribution of velocities, the collision rate coefficients given by the central field model and the Su and Chesnavich parametrization are proportional to $\mu^{-1/2}$. In Fig. 6, we show the collision rate coefficients as a function of $\mu^{-1/2}$ for all systems, from molecular dynamics trajectory simulations (MD), the central field model using the attractive potential fitted to the PMF (CF), and the Su and Chesnavich parametrization (SC). Strikingly, for systems where H_2SO_4 is the neutral collision partner, the collision rate coefficients are almost exactly proportional to $\mu^{-1/2}$. For the three collisions involving $[HSO_4^- \cdot (CH_3)_2NH_2^+]$, where the differences between β_{MD} and β_{CF}, and β_{SC} are more pronounced, a somewhat linear trend with $\mu^{-1/2}$ is still observed. Thus, the main property of the ion affecting β is its mass. This simple correlation between β and μ is rather unexpected due to the notable difference in the interaction potential (presented in Fig. 3). For the central field model, the results suggest that the effect of different interaction parameters (A, a and r_0) is balanced out in Eqs. (5) and (6), which is reflected in the very similar collision cross sections for the different ion–H_2SO_4 systems presented in Fig. 4(e–h), even though their underlying interaction parameters differ from each other, as shown in Tab. 1. Further research is needed to determine the underlying reason for this invariance.

Table 2. Collision rate coefficients obtained from molecular dynamics collision simulations β_{MD}, central field model with interaction parameters fitted to the PMF curve β_{CF}, Langevin-Gioumousis-Stevenson model β_{L}, and Su and Chesnavich (1982) parametrization β_{SC}, for all studied systems in 10^{-15} m^{3}s^{-1}.

System	β_{MD}	β_{CF}	$\beta_{\mathrm{MD}}/\beta_{\mathrm{CF}}$	β_{L}	$\beta_{\mathrm{MD}}/\beta_{\mathrm{L}}$	β_{SC}	$\beta_{\mathrm{MD}}/\beta_{\mathrm{SC}}$
$H_2SO_4 - HSO_4^-$	2.62	2.51	1.04	0.81	3.21	2.17	1.20
$H_2SO_4 - (CH_3)_2NH_2^+$	3.01	3.28	0.92	1.02	2.96	2.71	1.11
$H_2SO_4 - NH_4^+$	4.43	4.23	1.05	1.46	3.04	3.89	1.14
$H_2SO_4 - NO_3^-$	2.85	2.73	1.04	0.92	3.09	2.46	1.16
$H_2SO_4 - [H_2SO_4 \cdot HSO_4^-]$	2.18	2.21	0.98	0.70	3.10	1.88	1.16
$[HSO_4^- \cdot (CH_3)_2NH_2^+] - HSO_4^-$	9.50	10.25	0.93	0.72	13.15	6.83	1.39
$[HSO_4^- \cdot (CH_3)_2NH_2^+] - (CH_3)_2NH_2^+$	11.62	12.91	0.90	0.93	12.48	8.80	1.32
$[HSO_4^- \cdot (CH_3)_2NH_2^+] - [H_2SO_4 \cdot HSO_4^-]$	7.50	7.40	1.01	0.60	12.40	5.72	1.31

3.4 Temperature dependence

To study the temperature dependence of the collision kinetics, and the extent to which this is captured by the theoretical

335 models, we performed additional MD trajectory simulations and PMF calculations, for the H_2SO_4–HSO_4^- system at $T = 200$ and 400 K. Figure 7 shows the PMFs at different temperatures, along with the fits of the attractive interactions for the central field model at the given temperature. Over the temperature range considered, the position of the energy minimum (r_0) remains unaffected, which implies that the binding mechanism remains the same in this temperature range. The depth of the potential well, on the other hand, decreases with increasing temperature, and the changes in the shape of the potentials are reflected in
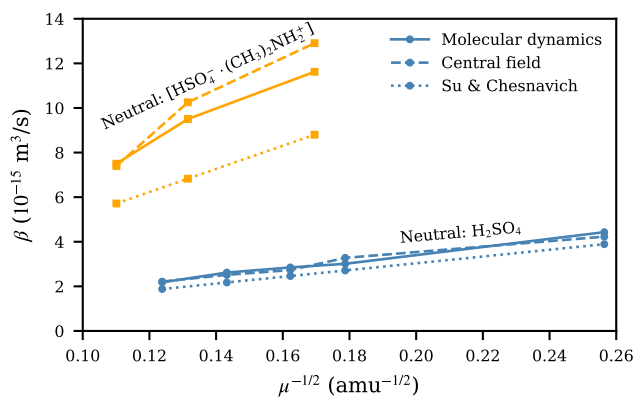

Figure 6. Collision rate coefficient β plotted as a function of $1/\sqrt{\mu}$ for collisions involving H_2SO_4 or $[HSO_4^- \cdot (CH_3)_2NH_2^+]$, from molecular dynamics trajectory simulations, the central field model using the attractive potential fitted to the PMF, and the Su and Chesnavich (1982) parametrization.
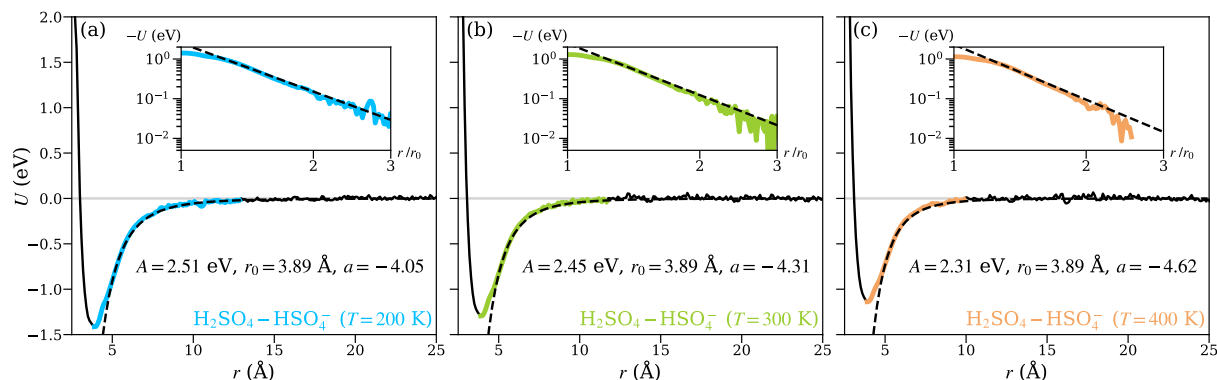
Figure 7. The potential of mean force (PMF) along the center-of-mass distance between the collision partners for the H_2SO_4–HSO_4^- system at temperatures (a) 200 K, (b) 300 K, and (c) 400 K. The solid black lines show the PMF curves obtained from well-tempered metadynamics simulations. The range over which the attractive interaction is fitted using Eq. (1) is highlighted in color, and shown on a logarithmic scale in the insets. The fits are shown as dashed black lines.

340 a small, but significant, decrease of the values of the parameters A and a. The almost linear dependence of the well depth on temperature is mostly due to increasing thermal motion in the molecules' rotational and vibrational degrees of freedom.

Figure 8(a) shows the collision cross sections obtained from MD simulations using different equilibration temperatures, sampling the relevant (v_0, b)-space (at $T = 400$ K, the relative velocity range was extended from 1000 to 1100 ms^{-1} to cover a wider velocity distribution). The central field model, using the fits to the PMFs at different temperatures, agrees with the

345 collision cross sections from MD simulations, and presents a similar narrowing trend of the cross sections with increasing temperature. The agreement is especially good at $T = 200$ K, but slightly worsens as temperature increases. The temperature dependence of the collision cross sections shows that the thermal energy of the colliding partners significantly affects the actual collision trajectories, and this effect is well captured by the changes in the potentials of mean force at different temperatures.

Due to the temperature dependence of the PMFs, correct collision rate coefficients cannot be computed by simply temperature-

350 scaling β_{CF} according to the Maxwell-Boltzmann distribution while using fixed parameters A and a obtained at a certain reference temperature. This is shown in Fig. 8(b), where the temperature dependencies of scaled β_{CF} (solid lines), based on the three PMF calculations at different temperatures are shown alongside the β_{MD} results (markers) at these temperatures. While Eq. (6) predicts a small positive temperature dependence for $a \lesssim -4$, the collision rate coefficients from MD simulations show that the actual dependence is stronger and negative. Scaling collision rate coefficients obtained from PMFs at a specific temper-

355 ature to other temperatures thus leads to significant discrepancies. In contrast, when using parameters from PMF calculations performed at the correct temperature, the central field model does predict a similar trend for collision rate coefficients as the MD simulations, as shown in Fig. 8(b). The agreement worsens at higher temperatures, with $\beta_{\mathrm{MD}}/\beta_{\mathrm{CF}}$ becoming about 1.14 at $T = 400$ K. Finally, while the Su and Chesnavich parametrization systematically underestimates the collision rate coefficients, the temperature dependence shows a similar trend as in the MD simulations over the range of temperatures considered. This
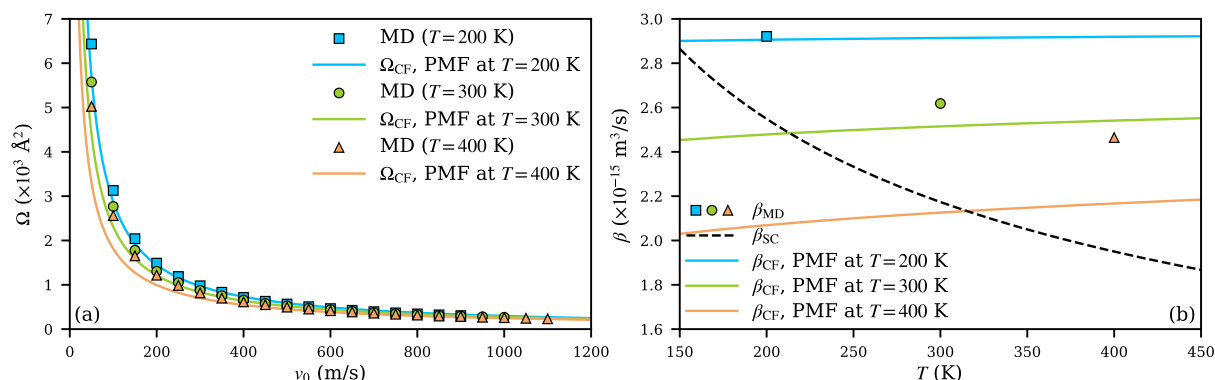
Figure 8. The collision cross section Ω (a) and collision rate coefficient β (b) of the H_2SO_4-HSO_4^- system at temperatures 200 K (blue), 300 K (green), and 400 K (orange). Results are shown as squares, circles, and triangles at the respective temperatures for MD simulations, as solid lines for the central field model, and as a dashed line for the Su and Chesnavich (1982) model.

360   good qualitative performance is due to the fact that the parametrization is based on trajectory calculations and thus is able to describe the fundamental dynamical effects adequately, if not the detailed interactions between actual molecules.

4   Conclusions

A proper theoretical treatment of bimolecular reactions requires an accurate assessment of the intermolecular potential. In the context of atmospheric clusters and their formation, high-level *ab initio* calculations are necessary for assessing the clusters'

365   stability in equilibrium (Elm et al., 2020). However, collision processes are governed by a centrifugal barrier located at larger intermolecular distances, where the strength of the interaction between colliding partners can be described with satisfactory accuracy and very small computational cost using classical force fields. In this study we have demonstrated the ability of different modelling approaches to describe the collision dynamics of ion-dipole systems in the free molecular regime.

The demand for accurate theoretical modelling of collisions between atmospheric molecules and clusters (neutral or charged)

370   arises from several recent observations and considerations: (1) At polluted sites, new particle formation (NPF) is controlled predominantly by collisions due to high vapor concentrations and extremely stable dimers (Kürten et al., 2014; Xiao et al., 2021). (2) Due to the immense improvement in *ab initio* calculations (Elm et al., 2020; Elm, 2020), the accuracy of current kinetic models used to predict atmospheric NPF rates is increasingly limited by the estimates for the collision rates, rather than the evaporation rates (Jiang et al., 2022). (3) In chemical ionization mass spectrometry, collisions between a studied

375   atmospheric cluster and a charging ion lead to the formation of a detectable charged cluster in the ionization chamber, while non-sticking collisions between the charged cluster and residual carrier gas in the atmospheric pressure interface can lead to cluster fragmentation causing systematic errors in the mass spectra (Zapadinsky et al., 2018). (4) One reason that ion-induced NPF is sometimes disregarded in global aerosol models is the lack of accurate rate coefficients for charged clusters (He et al., 2020).

380   While simple analytical and parametrized models exist for the calculation of collision rate coefficients of ion-dipole systems, these models do not directly account for the complexity encountered in molecular ions and dipoles, let alone dipolar or charged clusters. Thus, in this study we considered two fundamentally different modelling approaches to calculate ion-dipole collision rates of atmospheric molecules and clusters in the free molecular regime: molecular dynamics trajectory simulations and a central field model. Since accurate experimental data is currently missing for the investigated systems, the presented MD

385   simulations serve as reference as each collision trajectory evolves under the full set of atomistic interactions defined by the force field. In contrast, the motion of colliding particles in the central field model follows from the assumption that the effective interaction potential is close to isotropic and adiabatic, and thus provides an adequate analytical solution for a certain group of systems at specific conditions.

        In this work, we studied collisions of eight atmospherically relevant ion-dipole systems, described by an atomistic OPLS-

390   based force field. To achieve comparability between the MD simulations and the central field modelling, the attractive interaction in the central field model was fitted to the potentials of mean force between the collision partners, obtained from well-tempered metadynamics calculations at the respective temperature. The velocity-dependent collision cross sections from the central field model and the molecular dynamics simulations were found to be in excellent agreement, supporting the assumption that the process can be described by isotropic and adiabatic intermolecular dynamics. Furthermore, the cross sections

395   are very similar for systems with the same neutral dipole despite the differences in the underlying interaction potentials. Thus, we concluded that for the studied systems the canonical collision rate coefficients depend mostly on the dipole's properties while the ion affects only the velocity distribution, through its mass. This finding and the collision rate coefficients calculated from atomistic simulations are in good agreement with the widely used parametrization by Su and Chesnavich (1982) which is based on simplified trajectory simulations of point charges and polar rods and the classical (temperature-independent)

400   Langevin-Gioumousis-Stevenson (Langevin, 1905; Gioumousis and Stevenson, 1958) model. The dynamical correction given by the parametrization significantly improves the prediction of the Langevin-Gioumousis-Stevenson model, and the temperature dependence of the parametrization is found to be in qualitative agreement with the MD simulations. However, we found that the Su and Chesnavich (1982) parametrization predicts the collision rate coefficients less accurately for systems with a dimer as the dipolar collision partner. This inaccuracy may become even more pronounced for systems involving larger clusters,

405   which need to be investigated in future research.

        We have demonstrated that the combination of PMF calculation and central field model is a viable and elegant alternative to brute force sampling of collision trajectories over a large range of impact parameters and relative velocities, in particular for systems with long-ranged attractive interactions, such as between ions and dipoles in the gas-phase. The presented approaches will be used in the future to obtain the collision rate coefficients of a large group of molecules and clusters. The resulting

410   data will allow the assessment of the relative importance of particle growth pathways involving ions in the initial stages of atmospheric new particle formation (He et al., 2020).

Appendix A: *Ab initio* and force field calculations of dipole moments, and average polarizabilities

Ab initio values for the dipole moment and polarizability of H_2SO_4 and $[HSO_4^- \cdot (CH_3)_2NH_2^+]$ presented in Tab. A1 were obtained with the Gaussian 16 program (Frisch et al., 2016). Geometry optimizations were done with the ωB97X-D functional

415 (Chai and Head-Gordon, 2008) and the 6–31++G(d,p) basis set. The starting geometries for H_2SO_4 and $[HSO_4^- \cdot (CH_3)_2NH_2^+]$ were taken from the Atmospheric Cluster Database of Elm (2019).

For the force field model, the dipole moments μ_D of the collision partners studied in this work, reported in Tab. A1, were calculated for energy minimized configurations as

$$\mu_D = \left\| \sum_{i=1}^{N_c} (\mathbf{r}_i - \mathbf{r}_{com}) q_i \right\|, \tag{A1}$$

420 where N_c is the number of partial charges q_i with positions $\mathbf{r}_i$ in the compound, and $\mathbf{r}_{com}$ is the position of the compound's center of mass.

To determine the average polarizability of the compounds $\bar{\alpha}$, reported in Tab. A1, we applied electric fields E_j of different signs and magnitudes along the three Cartesian axes and performed an energy minimization of the system in LAMMPS (Plimpton, 1995), and recorded the resulting changes in the dipole moment components, $\Delta\mu_{D,i}$. We then performed linear fits

425 around $\|E_j\| = 0$ to obtain the components of the polarizability tensor as

$$\alpha_{ij} = \frac{\Delta\mu_{D,i}}{E_j}. \tag{A2}$$

After diagonalizing the polarizability tensor, the average polarizability was calculated from the diagonal elements as

$$\bar{\alpha} = \frac{1}{3}(\alpha_{11} + \alpha_{22} + \alpha_{33}). \tag{A3}$$

Appendix B: *Ab initio* and force field calculations of cluster binding energies

430 We benchmarked the accuracy of the all-atom OPLS force field in describing the structures and energies of stable clusters formed upon ion-dipole collision against *ab initio* calculations.

Ab initio single-point energies of all collision partners, and clusters formed after collision, were obtained from the Atmospheric Cluster Database of Elm (2019), except for NO_3^-, $H_2SO_4 - NO_3^-$, and $[HSO_4^- \cdot (CH_3)_2NH_2^+] - (CH_3)_2NH_2^+$, as these were not available from the database. The geometries of the compounds in the database were optimized using the ωB97X-D

435 functional (Chai and Head-Gordon, 2008) and the 6–31++G(d,p) basis set in the Gaussian 09, rev. D.01 program (Frisch et al., 2013). A single point energy calculation using the DLPNO-CCSD(T) (Riplinger and Neese, 2013; Riplinger et al., 2013) with an aug-cc-pVTZ basis set and normal PNO settings (Liakos et al., 2015) was then performed on this optimized geometry.

For consistency with the single point energy values obtained from the database, we followed a similar procedure for NO_3^-, $H_2SO_4 - NO_3^-$, and $[HSO_4^- \cdot (CH_3)_2NH_2^+] - (CH_3)_2NH_2^+$. First, to identify the lowest free energy conformer of the $H_2SO_4 -$

440 NO_3^- and $[HSO_4^- \cdot (CH_3)_2NH_2^+] - (CH_3)_2NH_2^+$ clusters, we used the JKCS configurational sampling procedure outlined by

Table A1. Dipole moments $\mu_{\mathrm{D}}^{\mathrm{OPLS}}$ and average polarizabilities $\bar{\alpha}^{\mathrm{OPLS}}$ of the chemical compounds used in the ion-dipole collision studies, as described by the all-atom OPLS force field. For charged compounds, the dipole moment is reported with respect to the compound's center of mass. For the neutral compounds, dipole moments $\mu_{\mathrm{D}}^{\mathrm{QM}}$ and average polarizabilities $\bar{\alpha}^{\mathrm{QM}}$ from *ab inito* calculation are provided for comparison.

Compound	$\mu_{\mathrm{D}}^{\mathrm{OPLS}}$ (Debye)	$\mu_{\mathrm{D}}^{\mathrm{QM}}$ (Debye)	$\bar{\alpha}^{\mathrm{OPLS}}$ ($\mathring{\mathrm{A}}^3$)	$\bar{\alpha}^{\mathrm{QM}}$ ($\mathring{\mathrm{A}}^3$)
H_2SO_4	3.17	3.27	6.57	4.91
$[HSO_4^- \cdot (CH_3)_2NH_2^+]$	13.20	8.97	7.91	10.13
HSO_4^-	4.41			
NO_3^-	0.00			
NH_4^+	0.00			
$(CH_3)_2NH_2^+$	1.84			
$[H_2SO_4 \cdot HSO_4^-]$	4.92			

Conversion between cgs and SI units of polarizability:
$1\,\mathring{\mathrm{A}}^3 = 1.1126 \times 10^{-40}\,\mathrm{Cm}^2\mathrm{V}^{-1}$.

Kubečka et al. (2019). In this procedure, all possible conformers and conjugate acids and bases of the molecules in the cluster are included as rigid monomers. Every combination of these rigid monomers that satisfies the cluster composition and total charge is then determined. Using the genetic algorithm of the ABCluster program (Zhang and Dolg, 2015), we created 300 conformers of each of these combination by starting from a population of 4000, performing 100 genetic steps, and keeping

445 the 300 conformers lowest in energy. The resulting conformers were optimized with the GFN–xTB semi-empirical method (Grimme et al., 2017). After this optimization, duplicates were removed and all remaining conformers with electronic energy less than 20 kcal/mol above the lowest energy conformer at the GFN–xTB level of theory were further optimized, along with a calculation of their vibrational frequencies, using the ωB97X-D functional and the 6–31++G(d,p) basis set in the Gaussian 16 program (Frisch et al., 2016). Of the three lowest free energy cluster conformers at the ωB97X-D level of theory, we performed

450 a single point energy calculation, employing DLPNO-CCSD(T) with an aug-cc-pVTZ basis set and normal PNO settings, as was done for the Elm database. To calculate the binding energies, the DLPNO-CCSD(T) single-point energy of the conformer with the lowest Gibbs free energy, calculated as $G = E^{\mathrm{DLPNO}} + G_{\mathrm{corr}}^{\omega\mathrm{B97X-D}}$, was used.

We used the global minimum energy configurations obtained from the *ab initio* calculations and performed an energy minimization with the all-atom OPLS force field in LAMMPS. For all compounds and clusters, the differences between the

455 re-optimized geometry and the *ab initio* reference structure were quite small, even for the larger clusters.

The cluster binding energies from *ab initio* and using the OPLS force field reported in Tab. B1 are given as the difference between the energy of the formed cluster and the energies of the original collision partners. The energies are overall in quite good agreement, with the force field typically predicting slightly weaker binding energies. The average unsigned error for all eight systems is 0.21 eV, and the largest difference of +0.55 eV was observed for the $[HSO_4^- \cdot (CH_3)_2NH_2^+] - HSO_4^-$

Table B1. Binding energies of collision systems obtained from *ab initio* calculations, ΔE_{QM} and using the OPLS force field, ΔE_{OPLS}, as well as the well depth of the potential of mean at $T = 300$ K, ΔU_{PMF}.

System	ΔE_{QM} (eV)	ΔE_{OPLS} (eV)	ΔU_{PMF} (eV)	$(\Delta E_{OPLS} - \Delta E_{QM})$ (eV)
$H_2SO_4 - HSO_4^-$	-2.04	-1.70	-1.29	$+0.34$
$H_2SO_4 - (CH_3)_2NH_2^+$	-0.84	-0.72	-0.51	$+0.12$
$H_2SO_4 - NH_4^+$	-0.92	-0.77	-0.56	$+0.15$
$H_2SO_4 - NO_3^-$	-2.01	-1.77	-1.34	$+0.24$
$H_2SO_4 - [H_2SO_4 \cdot HSO_4^-]$	-1.28	-1.42	-1.00	-0.14
$[HSO_4^- \cdot (CH_3)_2NH_2^+] - HSO_4^-$	-1.93	-1.38	-1.41	$+0.55$
$[HSO_4^- \cdot (CH_3)_2NH_2^+] - (CH_3)_2NH_2^+$	-1.83	-1.80	-1.62	$+0.03$
$[HSO_4^- \cdot (CH_3)_2NH_2^+] - [H_2SO_4 \cdot HSO_4^-]$	-1.42	-1.30	-1.18	$+0.12$

460 system. The table also includes the well depth of the potential of mean force, ΔU_{PMF}, for each system obtained from the well-tempered metadynamics simulation at $T = 300$ K. Due to the inclusion of thermal motion and proper sampling of different cluster configurations, the values of ΔU_{PMF} are typically less negative than the binding energies ΔE_{OPLS} obtained using the same force field at $T = 0$ K. In the scope of the present study, we conclude that the OPLS all-atom force field provides an adequate representation of the individual collision partners as well as the formed clusters after collision.

465 *Author contributions.* IN, HV and BR planned the study. IN, RH and BR designed the simulation framework. IN carried out the ab initio calculations and IN and BR carried out the force field based molecular dynamics collision and well-tempered metadynamics simulations. RH provided the theoretical framework. IN, RH, and BR analyzed the simulation data, and wrote the first draft of the manuscript. All authors contributed to writing the final paper.

Competing interests. The authors declare that they have no conflict of interest.

References

475   Amelynck, C., Schoon, N., Kuppens, T., Bultinck, P., and Arijs, E.: A selected ion flow tube study of the reactions of H_3O^+, NO^+ and O_2^+ with some oxygenated biogenic volatile organic compounds, Int. J. Mass Spectrom., 247, 1–9, https://doi.org/10.1016/j.ijms.2005.08.010, 2005.

Barducci, A., Bussi, G., and Parrinello, M.: Well-Tempered Metadynamics: A Smoothly Converging and Tunable Free-Energy Method, Phys. Rev. Lett., 100, 020 603, https://doi.org/10.1103/PhysRevLett.100.020603, 2008.

480   Chai, J.-D. and Head-Gordon, M.: Long-range corrected hybrid density functionals with damped atom–atom dispersion corrections, Phys. Chem. Chem. Phys., 10, 6615–6620, https://doi.org/10.1039/B810189B, 2008.

Chesnavich, W. J., Su, T., and Bowers, M. T.: Ion-dipole collisions: recent theoretical advances, in: Kinetics of Ion-Molecule Reactions, edited by Ausloos, P. J., pp. 31–53, Springer, https://doi.org/10.1007/978-1-4613-2931-2, 1979.

Chesnavich, W. J., Su, T., and Bowers, M. T.: Collisions in a noncentral field: a variational and trajectory investigation of ion–dipole capture, 485   J. Chem. Phys., 72, 2641–2655, https://doi.org/10.1063/1.439409, 1980.

Clary, D. C.: Fast Chemical Reactions: Theory Challenges Experiment, Ann. Rev. Phys. Chem., 41, 61–90, https://doi.org/10.1146/annurev.pc.41.100190.000425, 1990.

Dugan Jr., J. V. and Magee, J. L.: Capture collisions between ions and polar molecules, J. Chem. Phys., 47, 3103–3112, https://doi.org/10.1063/1.1712359, 1967.

490   Elm, J.: An Atmospheric Cluster Database Consisting of Sulfuric Acid, Bases, Organics, and Water, ACS Omega, 4, 10 965–10 974, https://doi.org/10.1021/acsomega.9b00860, 2019.

Elm, J.: Toward a Holistic Understanding of the Formation and Growth of Atmospheric Molecular Clusters: A Quantum Machine Learning Perspective, J. Phys. Chem. A, 125, 895–902, https://doi.org/10.1021/acs.jpca.0c09762, 2020.

Elm, J., Kubečka, J., Besel, V., Jääskeläinen, M. J., Halonen, R., Kurtén, T., and Vehkamäki, H.: Modeling the formation and growth of 495   atmospheric molecular clusters: A review, J. Aerosol Sci., 149, 105 621, https://doi.org/10.1016/j.jaerosci.2020.105621, 2020.

Falcon-Rodriguez, C. I., Osornio-Vargas, A. R., Sada-Ovalle, I., and Segura-Medina, P.: Aeroparticles, Composition, and Lung Diseases, Front. Immunol., 7, https://doi.org/10.3389/fimmu.2016.00003, 2016.

Fernández-Ramos, A., Miller, J. A., Klippenstein, S. J., and Truhlar, D. G.: Modeling the Kinetics of Bimolecular Reactions, Chem. Rev., 106, 4518–4584, https://doi.org/10.1021/cr050205w, 2006.

500   Frisch, M. J., Trucks, G. W., Schlegel, H. B., Scuseria, G. E., Robb, M. A., Cheeseman, J. R., Scalmani, G., Barone, V., Petersson, G. A., Nakatsuji, H., Li, X., Caricato, M., Marenich, A. V., Bloino, J., Janesko, B. G., Gomperts, R., Mennucci, B., Hratchian, H. P., Ortiz, J. V., Izmaylov, A. F., Sonnenberg, J. L., Williams-Young, D., Ding, F., Lipparini, F., Egidi, F., Goings, J., Peng, B., Petrone, A., Henderson, T., Ranasinghe, D., Zakrzewski, V. G., Gao, J., Rega, N., Zheng, G., Liang, W., Hada, M., Ehara, M., Toyota, K., Fukuda, R., Hasegawa, J., Ishida, M., Nakajima, T., Honda, Y., Kitao, O., Nakai, H., Vreven, T., Throssell, K., Montgomery, Jr., J. A., Peralta, J. E., Ogliaro, F., 505   Bearpark, M. J., Heyd, J. J., Brothers, E. N., Kudin, K. N., Staroverov, V. N., Keith, T. A., Kobayashi, R., Normand, J., Raghavachari, K., Rendell, A. P., Burant, J. C., Iyengar, S. S., Tomasi, J., Cossi, M., Millam, J. M., Klene, M., Adamo, C., Cammi, R., Ochterski, J. W., Martin, R. L., Morokuma, K., Farkas, O., Foresman, J. B., and Fox, D. J.: Gaussian~09 Revision D.01, gaussian Inc. Wallingford CT, 2013.

Frisch, M. J., Trucks, G. W., Schlegel, H. B., Scuseria, G. E., Robb, M. A., Cheeseman, J. R., Scalmani, G., Barone, V., Petersson, G. A., 510   Nakatsuji, H., Li, X., Caricato, M., Marenich, A. V., Bloino, J., Janesko, B. G., Gomperts, R., Mennucci, B., Hratchian, H. P., Ortiz, J. V.,

Izmaylov, A. F., Sonnenberg, J. L., Williams-Young, D., Ding, F., Lipparini, F., Egidi, F., Goings, J., Peng, B., Petrone, A., Henderson, T., Ranasinghe, D., Zakrzewski, V. G., Gao, J., Rega, N., Zheng, G., Liang, W., Hada, M., Ehara, M., Toyota, K., Fukuda, R., Hasegawa, J., Ishida, M., Nakajima, T., Honda, Y., Kitao, O., Nakai, H., Vreven, T., Throssell, K., Montgomery, Jr., J. A., Peralta, J. E., Ogliaro, F., Bearpark, M. J., Heyd, J. J., Brothers, E. N., Kudin, K. N., Staroverov, V. N., Keith, T. A., Kobayashi, R., Normand, J., Raghavachari,

515   K., Rendell, A. P., Burant, J. C., Iyengar, S. S., Tomasi, J., Cossi, M., Millam, J. M., Klene, M., Adamo, C., Cammi, R., Ochterski, J. W., Martin, R. L., Morokuma, K., Farkas, O., Foresman, J. B., and Fox, D. J.: Gaussian~16 Revision C.01, gaussian Inc. Wallingford CT, 2016.

Georgievskii, Y. and Klippenstein, S. J.: Long-range transition state theory, J. Chem. Phys., 122, 194 103, https://doi.org/10.1063/1.1899603, 2005.

520   Gioumousis, G. and Stevenson, D. P.: Reactions of Gaseous Molecule Ions with Gaseous Molecules. V. Theory, J. Chem. Phys., 29, 294–299, https://doi.org/10.1063/1.1744477, 1958.

Gopalakrishnan, R. and Hogan Jr, C. J.: Determination of the Transition Regime Collision Kernel from Mean First Passage Times, Aerosol Sci. Technol., 45, 1499–1509, https://doi.org/10.1080/02786826.2011.601775, 2011.

Gordon, H., Kirkby, J., Baltensperger, U., Bianchi, F., Breitenlechner, M., Curtius, J., Dias, A., Dommen, J., Donahue, N. M., Dunne,

525   E. M., Duplissy, J., Ehrhart, S., Flagan, R. C., Frege, C., Fuchs, C., Hansel, A., Hoyle, C. R., Kulmala, M., Kürten, A., Lehtipalo, K., Makhmutov, V., Molteni, U., Rissanen, M. P., Stozkhov, Y., Tröstl, J., Tsagkogeorgas, G., Wagner, R., Williamson, C., Wimmer, D., Winkler, P. M., Yan, C., and Carslaw, K. S.: Causes and importance of new particle formation in the present-day and preindustrial atmospheres, J. Geophys. Res.: Atmospheres, 122, 8739–8760, https://doi.org/10.1002/2017JD026844, 2017.

Goudeli, E., Lee, J., and Hogan Jr, C. J.: Silica nanocluster binding rate coefficients from molecular dynamics trajectory calculations,

530   J. Aerosol Sci., p. 105558, https://doi.org/10.1016/j.jaerosci.2020.105558, 2020.

Grimme, S., Bannwarth, C., and Shushkov, P.: A Robust and Accurate Tight-Binding Quantum Chemical Method for Structures, Vibrational Frequencies, and Noncovalent Interactions of Large Molecular Systems Parametrized for All spd-Block Elements (Z = 1–86), Journal of Chemical Theory and Computation, 13, 1989–2009, https://doi.org/10.1021/acs.jctc.7b00118, 2017.

Halonen, R., Zapadinsky, E., Kurtén, T., Vehkamäki, H., and Reischl, B.: Rate enhancement in collisions of sulfuric acid molecules due to

535   long-range intermolecular forces, Atmos. Chem. Phys., 19, 13 355–13 366, https://doi.org/10.5194/acp-19-13355-2019, 2019.

Halonen, R., Neefjes, I., and Reischl, B.: Technical note on the efficiency of different thermostats for equilibrating molecules in the gas phase, in preparation, 2022.

He, X.-C., Iyer, S., Sipilä, M., Ylisirniö, A., Peltola, M., Kontkanen, J., Baalbaki, R., Simon, M., Kürten, A., Tham, Y. J., Pesonen, J., Ahonen, L. R., Amanatidis, S., Amorim, A., Baccarini, A., Beck, L., Bianchi, F., Brilke, S., Chen, D., Chiu, R., Curtius, J., Dada, L., Dias,

540   A., Dommen, J., Donahue, N. M., Duplissy, J., Haddad, I. E., Finkenzeller, H., Fischer, L., Heinritzi, M., Hofbauer, V., Kangasluoma, J., Kim, C., Koenig, T. K., Kubečka, J., Kvashnin, A., Lamkaddam, H., Lee, C. P., Leiminger, M., Li, Z., Makhmutov, V., Xiao, M., Marten, R., Nie, W., Onnela, A., Partoll, E., Petäjä, T., Salo, V.-T., Schuchmann, S., Steiner, G., Stolzenburg, D., Stozkhov, Y., Tauber, C., Tomé, A., Väisänen, O., Vazquez-Pufleau, M., Volkamer, R., Wagner, A. C., Wang, M., Wang, Y., Wimmer, D., Winkler, P. M., Worsnop, D. R., Wu, Y., Yan, C., Ye, Q., Lehtinen, K., Nieminen, T., Manninen, H. E., Rissanen, M., Schobesberger, S., Lehtipalo, K.,

545   Baltensperger, U., Hansel, A., Kerminen, V.-M., Flagan, R. C., Kirkby, J., Kurtén, T., and Kulmala, M.: Determination of the collision rate coefficient between charged iodic acid clusters and iodic acid using the appearance time method, Aerosol Sci. Technol., 55, 1–12, https://doi.org/10.1080/02786826.2020.1839013, 2020.

Jiang, S., Liu, Y.-R., Huang, T., Feng, Y.-J., Wang, C.-Y., Wang, Z.-Q., Ge, B.-J., Liu, Q.-S., Guang, W.-R., and Huang, W.: A universal deep learning-based framework towards fully ab initio simulation of atmospheric aerosol nucleation, Preprint available at Research Square

550   [https://doi.org/10.21203/rs.3.rs-1191188/v1], https://doi.org/10.21203/rs.3.rs-1191188/v1, 2022.

Jorgensen, W. L., Maxwell, D. S., and Tirado-Rives, J.: Development and Testing of the OPLS All-Atom Force Field on Conformational Energetics and Properties of Organic Liquids, J. Am. Chem. Soc., 118, 11 225–11 236, https://doi.org/10.1021/ja9621760, 1996.

Kirkby, J., Duplissy, J., Sengupta, K., Frege, C., Gordon, H., Williamson, C., Heinritzi, M., Simon, M., Yan, C., Almeida, J., Tröstl, J., Nieminen, T., Ortega, I. K., Wagner, R., Adamov, A., Amorim, A., Bernhammer, A.-K., Bianchi, F., Breitenlechner, M., Brilke, S., Chen,

555   X., Craven, J., Dias, A., Ehrhart, S., Flagan, R. C., Franchin, A., Fuchs, C., Guida, R., Hakala, J., Hoyle, C. R., Jokinen, T., Junninen, H., Kangasluoma, J., Kim, J., Krapf, M., Kürten, A., Laaksonen, A., Lehtipalo, K., Makhmutov, V., Mathot, S., Molteni, U., Onnela, A., Peräkylä, O., Piel, F., Petäjä, T., Praplan, A. P., Pringle, K., Rap, A., Richards, N. A. D., Riipinen, I., Rissanen, M. P., Rondo, L., Sarnela, N., Schobesberger, S., Scott, C. E., Seinfeld, J. H., Sipilä, M., Steiner, G., Stozhkov, Y., Stratmann, F., Tomé, A., Virtanen, A., Vogel, A. L., Wagner, A. C., Wagner, P. E., Weingartner, E., Wimmer, D., Winkler, P. M., Ye, P., Zhang, X., Hansel, A., Dommen, J., Donahue,

560   N. M., Worsnop, D. R., Baltensperger, U., Kulmala, M., Carslaw, K. S., and Curtius, J.: Ion-induced nucleation of pure biogenic particles, Nature, 533, 521–526, https://doi.org/10.1038/nature17953, 2016.

Kubečka, J., Besel, V., Kurtén, T., Myllys, N., and Vehkamäki, H.: Configurational Sampling of Noncovalent (Atmospheric) Molecular Clusters: Sulfuric Acid and Guanidine, J. Phys. Chem. A, 123, 6022–6033, https://doi.org/10.1021/acs.jpca.9b03853, 2019.

Kürten, A., Jokinen, T., Simon, M., Sipilä, M., Sarnela, N., Junninen, H., Adamov, A., Almeida, J., Amorim, A., Bianchi, F., Breitenlechner,

565   M., Dommen, J., Donahue, N. M., Duplissy, J., Ehrhart, S., Flagan, R. C., Franchin, A., Hakala, J., Hansel, A., Heinritzi, M., Hutterli, M., Kangasluoma, J., Kirkby, J., Laaksonen, A., Lehtipalo, K., Leiminger, M., Makhmutov, V., Mathot, S., Onnela, A., Petäjä, T., Praplan, A. P., Riccobono, F., Rissanen, M. P., Rondo, L., Schobesberger, S., Seinfeld, J. H., Steiner, G., Tomé, A., Tröstl, J., Winkler, P. M., Williamson, C., Wimmer, D., Ye, P., Baltensperger, U., Carslaw, K. S., Kulmala, M., Worsnop, D. R., and Curtius, J.: Neutral molecular cluster formation of sulfuric acid–dimethylamine observed in real time under atmospheric conditions, Proc. Natl. Acad. Sci. USA, 111,

570   15 019–15 024, https://doi.org/10.1073/pnas.1404853111, 2014.

Kurtén, T., Kulmala, M., Dal Maso, M., Suni, T., Reissell, A., Vehkamäki, H., Hari, P., Laaksonen, A., Viisanen, Y., and Vesala, T.: Estimation of different forest-related contributions to the radiative balance using observations in southern Finland, Boreal Environ. Res., 8, 275–285, 2003.

Langevin, P.: A fundamental formula of kinetic theory, Ann. Chim. Phys., 5, 245–288, 1905.

575   Liakos, D. G., Sparta, M., Kesharwani, M. K., Martin, J. M. L., and Neese, F.: Exploring the Accuracy Limits of Local Pair Natural Orbital Coupled-Cluster Theory, J. Chem. Theory Comput., 11, 1525–1539, https://doi.org/10.1021/ct501129s, 2015.

Loukonen, V., Bork, N., and Vehkamäki, H.: From collisions to clusters: first steps of sulphuric acid nanocluster formation dynamics, Mol. Phys., 112, 1979–1986, https://doi.org/10.1080/00268976.2013.877167, 2014.

Maergoiz, A., Nikitin, E., Troe, J., and Ushakov, V.: Classical trajectory and adiabatic channel study of the transition from adiabatic to sudden

580   capture dynamics. I. Ion–dipole capture, J. Chem. Phys., 105, 6263–6269, https://doi.org/10.1063/1.472480, 1996a.

Maergoiz, A., Nikitin, E., Troe, J., and Ushakov, V.: Classical trajectory and adiabatic channel study of the transition from adiabatic to sudden capture dynamics. II. Ion–quadrupole capture, J. Chem. Phys., 105, 6270–6276, https://doi.org/10.1063/1.472468, 1996b.

Maergoiz, A., Nikitin, E., Troe, J., and Ushakov, V.: Classical trajectory and adiabatic channel study of the transition from adiabatic to sudden capture dynamics. III. Dipole–dipole capture, J. Chem. Phys., 105, 6277–6284, https://doi.org/10.1063/1.472481, 1996c.

585 McGrath, M. J., Olenius, T., Ortega, I. K., Loukonen, V., Paasonen, P., Kurtén, T., Kulmala, M., and Vehkamäki, H.: Atmospheric Cluster Dy-
       namics Code: a flexible method for solution of the birth-death equations, Atmos. Chem. Phys., 12, 2345–2355, https://doi.org/10.5194/acp-
       12-2345-2012, 2012.

       Midey, A. J., Williams, S., and Viggiano, A. A.: Reactions of NO$^+$ with Isomeric Butenes from 225 to 500 K, J. Phys. Chem. A, 105,
       1574–1578, https://doi.org/10.1021/jp0019005, 2001.

590 Moran, T. F. and Hamill, W. H.: Cross Sections of Ion—Permanent-Dipole Reactions by Mass Spectrometry, J. Chem. Phys., 39, 1413–1422,
       https://doi.org/10.1063/1.1734457, 1963.

       Mosallanejad, S., Oluwoye, I., Altarawneh, M., Gore, J., and Dlugogorski, B. Z.: Interfacial and bulk properties of concentrated solutions of
       ammonium nitrate, Phys. Chem. Chem. Phys., 22, 27 698–27 712, https://doi.org/10.1039/D0CP04874G, 2020.

       Plimpton,   S.:   Fast   Parallel   Algorithms   for   Short-Range   Molecular   Dynamics,   J.   Comp.   Phys.,   117,   1–19,
595   https://doi.org/10.1006/jcph.1995.1039, 1995.

       Riplinger, C. and Neese, F.: An efficient and near linear scaling pair natural orbital based local coupled cluster method, J. Chem. Phys., 138,
       034 106, https://doi.org/10.1063/1.4773581, 2013.

       Riplinger, C., Sandhoefer, B., Hansen, A., and Neese, F.: Natural triple excitations in local coupled cluster calculations with pair natural
       orbitals, J. Chem. Phys., 139, 134 101, https://doi.org/10.1063/1.4821834, 2013.

600 Strekowski, R. S., Alvarez, C., Petrov-Stojanović, J., Hagebaum-Reignier, D., and Wortham, H.: Theoretical chemical ionization rate con-
       stants of the concurrent reactions of hydronium ions (H$_3$O$^+$) and oxygen ions (O) with selected organic iodides, J. Mass Spectrom., 54,
       422–428, https://doi.org/10.1002/jms.4349, 2019.

       Su, T. and Bowers, M. T.: Theory of ion-polar molecule collisions. Comparison with experimental charge transfer reactions of rare gas ions
       to geometric isomers of difluorobenzene and dichloroethylene, J. Chem. Phys., 58, 3027–3037, https://doi.org/10.1063/1.1679615, 1973.

605 Su, T. and Chesnavich, W. J.: Parametrization of the ion–polar molecule collision rate constant by trajectory calculations, J. Chem. Phys.,
       76, 5183–5185, https://doi.org/10.1063/1.442828, 1982.

       Su, T., Su, E. C., and Bowers, M. T.: Ion–polar molecule collisions. Conservation of angular momentum in the average dipole orientation
       theory. The AADO theory, J. Chem. Phys., 69, 2243–2250, https://doi.org/10.1063/1.436783, 1978.

       Thajudeen, T., Gopalakrishnan, R., and Hogan Jr., C. J.: The Collision Rate of Nonspherical Particles and Aggregates for all Diffusive
610   Knudsen Numbers, Aerosol Sci. Technol., 46, 1174–1186, https://doi.org/10.1080/02786826.2012.701353, 2012.

       Tribello, G. A., Bonomi, M., Branduardi, D., Camilloni, C., and Bussi, G.: Plumed 2: New feathers for an old bird, Comput. Phys. Commun.,
       185, 604–613, https://doi.org/10.1016/j.cpc.2013.09.018, 2014.

       Troe, J.: Statistical adiabatic channel model of ion-neutral dipole capture rate constants, Chem. Phys. Lett., 122, 425–430,
       https://doi.org/10.1016/0009-2614(85)87240-7, 1985.

615 Troe, J.: Statistical adiabatic channel model for ion–molecule capture processes, J. Chem. Phys., 87, 2773–2780,
       https://doi.org/10.1063/1.453701, 1987.

       Wagner, R., Yan, C., Lehtipalo, K., Duplissy, J., Nieminen, T., Kangasluoma, J., Ahonen, L. R., Dada, L., Kontkanen, J., Manninen, H. E.,
       Dias, A., Amorim, A., Bauer, P. S., Bergen, A., Bernhammer, A.-K., Bianchi, F., Brilke, S., Mazon, S. B., Chen, X., Draper, D. C.,
       Fischer, L., Frege, C., Fuchs, C., Garmash, O., Gordon, H., Hakala, J., Heikkinen, L., Heinritzi, M., Hofbauer, V., Hoyle, C. R., Kirkby,
620   J., Kürten, A., Kvashnin, A. N., Laurila, T., Lawler, M. J., Mai, H., Makhmutov, V., Mauldin III, R. L., Molteni, U., Nichman, L., Nie, W.,
       Ojdanic, A., Onnela, A., Piel, F., Quéléver, L. L. J., Rissanen, M. P., Sarnela, N., Schallhart, S., Sengupta, K., Simon, M., Stolzenburg,
       D., Stozhkov, Y., Tröstl, J., Viisanen, Y., Vogel, A. L., Wagner, A. C., Xiao, M., Ye, P., Baltensperger, U., Curtius, J., Donahue, N. M.,

Flagan, R. C., Gallagher, M., Hansel, A., Smith, J. N., Tomé, A., Winkler, P. M., Worsnop, D., Ehn, M., Sipilä, M., Kerminen, V.-M., Petäjä, T., and Kulmala, M.: The role of ions in new particle formation in the CLOUD chamber, Atmos. Chem. Phys., 17, 15 181–15 197,

625   https://doi.org/10.5194/acp-17-15181-2017, 2017.

Williams, S., Knighton, W. B., Midey, A. J., Viggiano, A. A., Irle, S., Wang, Q., and Morokuma, K.: Oxidation of Alkyl Ions in Reactions with O_2 and O_3 in the Gas Phase, J. Phys. Chem. A, 108, 1980–1989, https://doi.org/10.1021/jp031099+, 2004.

Woon, D. and Herbst, E.: Quantum chemical predictions of the properties of known and postulated neutral interstellar molecules, Astrophys. J., Suppl. Ser., 185, https://doi.org/10.1021/jp031099+, 2009.

630   Xiao, M., Hoyle, C. R., Dada, L., Stolzenburg, D., Kürten, A., Wang, M., Lamkaddam, H., Garmash, O., Mentler, B., Molteni, U., Baccarini, A., Simon, M., He, X.-C., Lehtipalo, K., Ahonen, L. R., Baalbaki, R., Bauer, P. S., Beck, L., Bell, D., Bianchi, F., Brilke, S., Chen, D., Chiu, R., Dias, A., Duplissy, J., Finkenzeller, H., Gordon, H., Hofbauer, V., Kim, C., Koenig, T. K., Lampilahti, J., Lee, C. P., Li, Z., Mai, H., Makhmutov, V., Manninen, H. E., Marten, R., Mathot, S., Mauldin, R. L., Nie, W., Onnela, A., Partoll, E., Petäjä, T., Pfeifer, J., Pospisilova, V., Quéléver, L. L. J., Rissanen, M., Schobesberger, S., Schuchmann, S., Stozhkov, Y., Tauber, C., Tham, Y. J., Tomé,

635   A., Vazquez-Pufleau, M., Wagner, A. C., Wagner, R., Wang, Y., Weitz, L., Wimmer, D., Wu, Y., Yan, C., Ye, P., Ye, Q., Zha, Q., Zhou, X., Amorim, A., Carslaw, K., Curtius, J., Hansel, A., Volkamer, R., Winkler, P. M., Flagan, R. C., Kulmala, M., Worsnop, D. R., Kirkby, J., Donahue, N. M., Baltensperger, U., El Haddad, I., and Dommen, J.: The driving factors of new particle formation and growth in the polluted boundary layer, Atmos. Chem. Phys., 21, 14 275–14 291, https://doi.org/10.5194/acp-21-14275-2021, 2021.

Yang, H., Goudeli, E., and Hogan Jr, C. J.: Condensation and dissociation rates for gas phase metal clusters from molecular dynamics

640   trajectory calculations, J. Chem. Phys., 148, 164 304, https://doi.org/10.1063/1.5026689, 2018.

Yu, F. and Luo, G.: Simulation of particle size distribution with a global aerosol model: contribution of nucleation to aerosol and CCN number concentrations, Atmos. Chem. Phys., 9, 7691–7710, https://doi.org/10.5194/acp-9-7691-2009, 2009.

Zapadinsky, E., Passananti, M., Myllys, N., Kurtén, T., and Vehkamäki, H.: Modeling on fragmentation of clusters inside a mass spectrometer, J. Phys. Chem. A, 123, 611–624, https://doi.org/10.1021/acs.jpca.8b10744, 2018.

645   Zhang, J. and Dolg, M.: ABCluster: the artificial bee colony algorithm for cluster global optimization, Phys. Chem. Chem. Phys., 17, 24 173–24 181, https://doi.org/10.1039/C5CP04060D, 2015.

Zhang, K., Feichter, J., Kazil, J., Wan, H., Zhuo, W., Griffiths, A. D., Sartorius, H., Zahorowski, W., Ramonet, M., Schmidt, M., Yver, C., Neubert, R. E. M., and Brunke, E.-G.: Radon activity in the lower troposphere and its impact on ionization rate: a global estimate using different radon emissions, Atmos. Chem. Phys., 11, 7817–7838, https://doi.org/10.5194/acp-11-7817-2011, 2011.

650   Zhao, J., Eisele, F. L., Titcombe, M., Kuang, C., and McMurry, P. H.: Chemical ionization mass spectrometric measurements of atmospheric neutral clusters using the cluster-CIMS, Journal of Geophysical Research: Atmospheres, 115, https://doi.org/10.1029/2009JD012606, 2010.